Quenched charge disorder in CuO_2 spin chains: Experimental and numerical studies

R. Leidl,[1] R. Klingeler,[2,3] B. Büchner,[3] M. Holtschneider,[1] and W. Selke[1]
[1]*Institut für Theoretische Physik, Rheinisch-Westfälische Technische Hochschule Aachen, 52056 Aachen, Germany*
[2]*Laboratoire National des Champs Magnétiques Pulsés, 31432 Toulouse, France*
[3]*Leibniz Institute for Solid State and Materials Research IFW Dresden, 01171 Dresden, Germany*
(Received 10 March 2006; published 13 June 2006)

We report on measurements of the magnetic response of the anisotropic CuO_2 spin chains in lightly hole-doped $La_x(Ca,Sr)_{14-x}Cu_{24}O_{41}$, $x \gtrsim 5$. The experimental data suggest that in magnetic fields $B \gtrsim 4$ T (applied along the easy axis) the system is characterized by short-range spin order and quasistatic (quenched) charge disorder. The magnetic susceptibility $\chi(B)$ shows a broad anomaly, which we interpret as the remnant of a spin-flop transition. To corroborate this idea, we present Monte Carlo simulations of a classical, anisotropic Heisenberg model with randomly distributed, static holes. Our numerical results clearly show that the spin-flop transition of the pure model (without holes) is destroyed and smeared out due to the disorder introduced by the quasistatic holes. Both the numerically calculated susceptibility curves $\chi(B)$ and the temperature dependence of the position of the anomaly are in qualitative agreement with the experimental data.

DOI: 10.1103/PhysRevB.73.224415 PACS number(s): 75.25.+z, 75.10.Hk, 74.72.Dn, 05.10.Ln

I. INTRODUCTION

The tendency of charge carriers for self-organization seems to be an intrinsic property of hole-doped transition metal oxides. One remarkable example which emphasizes the interplay of charge order and antiferromagnetism is the formation of spatial spin and charge modulations in the high-T_c cuprates.[1] Other examples for self-organization of holes in low-dimensional magnets include the layered nickelates[2,3] and manganites,[4] and the doped CuO_2 spin chain systems such as $Sr_{14-x}Ca_xCu_{24}O_{41}$ and $Na_{1+x}CuO_2$.[5–8] On the other hand, these observations also suggest that quenched disorder plays an important role in such systems. In the case of the half-doped manganites, the quenched structural A-site disorder was found to enhance the fluctuations of the competing order parameters, i.e., between the charge/orbital order and the metallic ferromagnetism.[9] The example of the manganites shows that, in the case of competing phases, quenched disorder can lead to properties that are very different from those of a slightly impure material.[10] Quenched disorder can also significantly affect the properties of hole-doped layered cuprates.[11] For example, recent numerical results suggest that disorder effects are important to describe the underdoped regime of the layered cuprates and the pseudogap in these compounds.[12]

In this paper, we report on experimental and numerical studies of the magnetic response of a cuprate model system, i.e., the lightly hole-doped CuO_2 spin chains in $La_x(Ca,Sr)_{14-x}Cu_{24}O_{41}$, with $x \gtrsim 5$. In these compounds, two quasi-one-dimensional (1D) magnetic structures are realized: Cu_2O_3 spin ladders and CuO_2 spin chains. The former exhibit a large spin gap of $\Delta_{gap} \sim 400$ K.[13] Hence the magnetic response at low temperature, which is the subject of our study, is due to the chains. The chains consist of edge-sharing CuO_4 plaquettes containing Cu^{2+} ions with spin $S=1/2$ and nonmagnetic Zhang-Rice singlets. The concentration of holes in the spin chains amounts to less than 10% and the Cu spins in the hole-free chain segments form predominantly ferromagnetic (FM) fragments since the nearest-neighbor (NN) coupling is ferromagnetic. The NN coupling is anisotropic, thereby causing an uniaxial anisotropy perpendicular to the CuO_4-plaquettes, i.e., along the crystallographic b axis.[14,15] In contrast, the magnetic coupling of Cu spins via a hole is antiferromagnetic (AFM), as is known from a comparison with the strongly (i.e., 60%) hole-doped spin chains of the mother compound $Sr_{14}Cu_{24}O_{41}$.[16,17] Moreover, there is a finite interchain coupling causing 3D AFM spin order below $T_N \sim 10$ K.[18,19] In previous papers we have argued that the spin ordered phase at zero magnetic field is presumably also characterized by a (short-range) charge order.[20,21] External magnetic fields of the order of a few Tesla suppress the long-range spin order when applied along the easy axis and cause a short-range antiferromagnetically spin ordered and charge disordered phase.[19,21] In the present paper we concentrate on the properties of the intermediate field phase at several Tesla, which is characterized by (i) short-range AFM spin order, and (ii) quasistatic charge disorder.

II. MOTIVATION OF THE MODEL

As was shown previously, the melting of long-range AFM spin order at a field $B=B_1$ (depending on temperature) causes an anomaly in the magnetization $M(B)$.[19,21] This is demonstrated by Fig. 1(a), which shows the magnetization $M(B)$, at fixed temperature $T=2.5$ K, of $La_{5.2}Ca_{8.8}Cu_{24}O_{41}$. If the magnetic field is oriented parallel to the chain direction, i.e., $B \| c$, the magnetization depends linearly on B, except for a small contribution of free spins. In contrast, two anomalies are observed in $M(B \| b)$, which become clearly visible if the susceptibility $\chi = \partial M / \partial B$ in Fig. 1(b) is considered. At $B_1 = 3.75$ T one recognizes a sharp peak which is attributed to the melting of the long-range spin order. Hence this anomaly signals a transition from a spin and (probably short-ranged) charge ordered phase for low fields $B \| b < B_1$ into a charge disordered state for $B > B_1$.

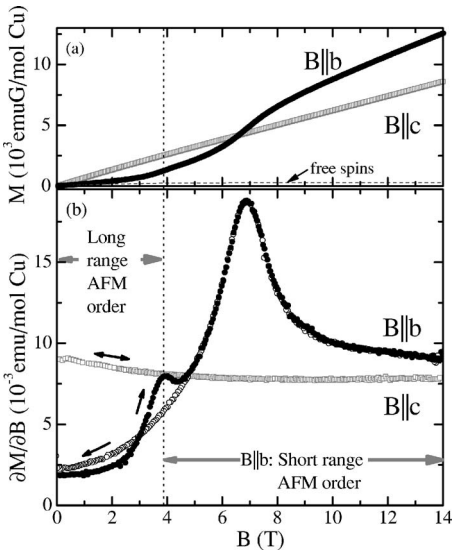

FIG. 1. Magnetization M (a), and susceptibility $\chi=\partial M/\partial B$ (b), of $La_{5.2}Ca_{8.8}Cu_{24}O_{41}$, at $T=2.5$ K vs magnetic field B parallel to the b- and to the c-axis, respectively (Ref. 21). The data are corrected by the g-factor taken from Ref. 15. In (a), the small, isotropic contribution due to free defect spins (dashed curve) has been subtracted, see Ref. 22. The vertical dashed line shows the phase boundary between long-range and short-range antiferromagnetic spin order.

Based on the suggestions described in Ref. 22, various theoretical studies have been devoted to the phenomena at $B=B_1$.[20,23–25] There the magnetic degrees of freedom were described by Ising spins and the holes were assumed to move either freely along the chains or under the influence of a periodic pinning potential stabilizing a striped structure. These models predict a breakdown of the striped (charge ordered) phase and may thus explain the transition at $B=B_1$.

Our present study, however, focuses on the properties for $B>B_1$. Previous numerical and experimental work[20–22] implies that this phase is characterized by short-range AFM spin correlations and quasistatic (quenched) charge disorder. The data in Fig. 1(b) display an additional broad peak in χ, at $B_2=6.9\ \mathrm{T}>B_1$, which was not captured by the previous theoretical studies. We attribute this anomaly to the reorientation of the Cu spins. The idea that the anomaly at B_2 is in fact a "smoothened out" spin-flop transition will be explored in greater detail in the next section, where we present the results of our Monte Carlo simulations. We propose that the anomaly at $B=B_2$ is the relic of a spin-flop transition, which is smeared out due to the strong disorder induced by the quasistatic holes. In this sense one may call the anomaly a "pseudo" spin-flop peak.

In the scenario of the "pseudo" spin-flop transition, the magnetic field overcomes, for $B>B_2$, the uniaxial anisotropy which is due to the nearly 90° Cu-O-Cu exchange (cf. Refs. 14 and 15). Quantitatively, the experimental value of B_2 is consistent with a recent inelastic neutron scattering study on $La_5Ca_9Cu_{24}O_{41}$,[26] which reported a spin gap of $\Delta_{\mathrm{gap}}/(g\mu_B)=(7\pm0.5)\mathrm{T}$.

III. NUMERICAL SIMULATIONS

A. Definition of the model, choice of interaction parameters, and simulation method

Taking the scenario of quenched charge disorder and short-range AFM spin order for $B>B_1$ as our starting point, we adopt a complementary view to the previous studies which considered mobile charge carriers and study the influence of *quenched* charge disorder on the magnetic properties of the system, ignoring the mobility of the holes altogether.

We consider a $L\times L$ square lattice consisting of L rows, which we identify with the chains, and L sites per chain. This choice of lattice geometry is motivated by neutron scattering experiments indicating that the copper ions in the CuO_2 planes of $La_5Ca_{14}Cu_{24}O_{41}$ form a rectangular array.[27] We conveniently set the lattice constants along and perpendicular to the chains equal to unity. Periodic boundary conditions are employed throughout.

Each site (i,j), where i is the chain index and j labels the sites along the chain, is either occupied by a spin (representing a magnetic Cu^{2+} ion), or a nonmagnetic hole (Zhang-Rice singlet). To describe the hole distribution, we introduce random variables $p_{i,j}$ taking the values $p_{i,j}=1$ if a spin resides at lattice site (i,j) and $p_{i,j}=0$ if it is occupied by a hole. The spins are modeled by (classical) three-component vectors $\vec{S}_{i,j}=(S^x_{i,j},S^y_{i,j},S^z_{i,j})$ with $|\vec{S}_{i,j}|=1$. As discussed in Ref. 28, we expect our results to remain qualitatively correct if one took the quantum character of the spins properly into account (although there would be, of course, quantitative deviations). This is basically a consequence of the Ising-like anisotropy of the model which tends to suppress quantum fluctuations, in particular in the presence of a field applied along the easy axis as in our case. If a hole is at site (i,j), we set $\vec{S}_{i,j}=0$. We simulate either the pure system without holes ($p_{i,j}=1$ for all i,j), or employ a fixed hole concentration of 10% within each chain. The latter should resemble the situation in the lightly hole-doped chain systems of $La_xCa_{14-x}Cu_{24}O_{41}$ with $x\sim5$. Moreover, we disallow nearest-neighbor pairs of holes within the same chain, since such configurations are energetically unfavorable due to the strong Coulomb repulsion. Thus consecutive holes along the chains are always separated by at least one spin.

The configurational energy depends both on the spin variables $\{\vec{S}_{i,j}\}$ and the hole distribution described by the occupation variables $\{p_{i,j}\}$. In a field H applied along the z-axis, the Hamiltonian of our model reads:

$$\mathcal{H}=-J_{c1}\sum_{i,j}(\vec{S}_{i,j}\cdot\vec{S}_{i,j+1}+\Delta S^z_{i,j}S^z_{i,j+1})-J_{c2}\sum_{i,j}\vec{S}_{i,j}\cdot\vec{S}_{i,j+2}$$
$$-J_0\sum_{i,j}(1-p_{i,j+1})\vec{S}_{i,j}\cdot\vec{S}_{i,j+2}-J_a\sum_{i,j}\vec{S}_{i,j}\cdot\vec{S}_{i+1,j}-H\sum_{i,j}S^z_{i,j}. \quad (1)$$

The interactions of this model are shown schematically in Fig. 2. The Cu-O-Cu bonding angle of nearly 90° suggests that the nearest-neighbor (NN) intrachain coupling J_{c1} is ferromagnetic ($J_{c1}>0$). Moreover, this coupling is anisotropic,[14,15,19] favoring the alignment of the spins along

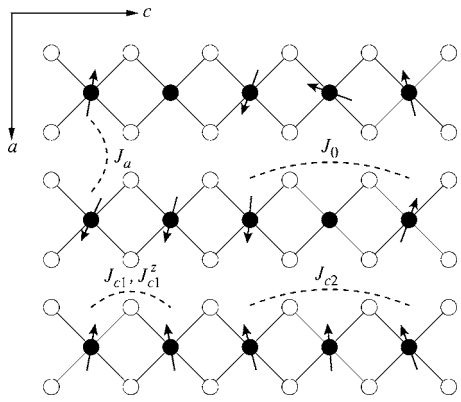

FIG. 2. Schematic representation of the interactions of our model Hamiltonian, Eq. (1). Closed and open circles denote Cu and O atoms, respectively. Nearest-neighbor (NN) spins along the CuO_2 chains (c direction) interact via an anisotropic ferromagnetic exchange [$J_{c1}, J_{c1}^z=(1+\Delta)J_{c1}$], whereas next-nearest-neighbor (NNN) spins are coupled antiferromagnetically. The strength of the antiferromagnetic coupling depends on whether the NNN spins are separated by a hole (J_0) or by another spin (J_{c2}). Finally, neighboring chains have an AFM interaction (J_a).

an easy axis (the crystallographic b-axis), which we take to be the z-axis. The anisotropy parameter is $\Delta>0$, where $\Delta=0$ corresponds to the isotropic case. In CuO_2 spin chains one expects next-nearest-neighbor (NNN) spins to be coupled antiferromagnetically.[29] The coupling between NNN spins is $J_{c2}<0$ if they are separated by a spin and $J_0<0$ if a hole resides between them, where $|J_0|>|J_{c2}|$. The difference is mainly caused by the smaller size of the Cu^{3+} ions leading to a stronger overlap of the p-orbitals of the involved oxygen ions. Finally, in accordance with the experimentally observed long-range AFM ordering, we assume an interchain coupling $J_a<0$ between NN spins on adjacent chains.

In the following, we turn to the values of the interaction parameters of Eq. (1). To the best of our knowledge, no direct information on the magnetic coupling parameters is available which agrees with our thermodynamic studies.[30] Thus for the numerical simulations we indirectly estimate the interaction parameters. First, we address the NNN interaction across a hole. This parameter has been determined to be $J_0/k_B=-130$ K from neutron diffraction studies of the stoichiometric compound $Sr_{14}Cu_{24}O_{41}$.[16,31] In contrast to J_0, only little is known about J_{c1} and J_{c2}. Qualitatively, the bonding geometry suggests $J_{c1}>0$ and $J_{c2}<0$.[14,32,33] In addition, the presence of ferromagnetic spin order along the chains in the weakly hole-doped compounds implies $|J_{c1}|>|J_{c2}|$. In order to get a quantitative estimation, we apply the exchange parameters which have been extracted for the undoped CuO_2 spin chains in Li_2CuO_2. In this compound, the Cu-O-Cu bonding angles in the CuO_2 spin chains are very similar to those of $(Ca,Sr)_{14-x}La_xCu_{24}O_{41}$. Thus we take $J_{c1}/k_B=100$ K.[33–35] Moreover, we assume $J_{c2}/k_B=-35$ K, which is again estimated from a comparison with Li_2CuO_2 by applying the bond-valence sum rule and the pressure dependence of J_0 in $Sr_{14}Cu_{24}O_{41}$. For $Sr_{14}Cu_{24}O_{41}$, the latter amounts to $\partial J_0/\partial p_c=4.2$ K/GPa.[17]

The magnitude of J_a significantly affects the zero-field ordering temperature of the model (without holes). In $Sr_{14}Cu_{24}O_{41}$, the coupling between Cu spins in adjacent chains amounts to $J_a\simeq-20$ K.[16] However, preliminary diffraction experiments[27] suggest changes of the relative positions of neighboring CuO_2 chains upon La-doping, which are supposed to strongly affect the interchain coupling constant. According to a recent result on undoped spin chains in Ref. 32,

$$\Theta_{\mathrm{CW}}^{\mathrm{3D}} \approx \Theta_{\mathrm{CW}}^{\mathrm{1D}} - z_{\mathrm{eff}}\frac{J_a}{4}, \tag{2}$$

where the 3D Curie-Weiss temperature may be estimated as $\Theta_{\mathrm{CW}}^{\mathrm{3D}}\simeq-8$ K from a fit to high-temperature susceptibility data,[22] while for the 1D Curie-Weiss temperature one has $\Theta_{\mathrm{CW}}^{\mathrm{1D}}\simeq 0.23J_{c1}=-23$ K from a cluster calculation.[32] Using the (approximate) effective number $z_{\mathrm{eff}}=2$ of nearest neighbors at surrounding chains, one gets a slightly larger value $J_a\simeq-30$ K as compared to $Sr_{14}Cu_{24}O_{41}$. This estimate, however, intimately depends on z_{eff}, which might be different. In the following, we set $J_a/k_B=-25$ K, since this gives rise to a zero-field ordering temperature which appears to be quite reasonable as compared to the experiments (see the discussion in Sec. III B).

From the interaction parameters J_{c1}, J_{c2}, and J_a, and a fit to the experimentally determined spin-wave gap of Ref. 26, we can calculate the anisotropy parameter Δ. This yields $\Delta=0.0255$.

The model is simulated employing a single-spin Metropolis algorithm. System sizes range from $L=20$ to 240. To obtain good equilibrium data, up to 2×10^7 Monte Carlo steps per site are needed for the largest systems. At the beginning of each run, 20% of the steps are discarded for thermalization. For the system with holes, we average over up to 300 randomly generated realizations of the disorder.

A quantity of primary concern due to its relation to the experiments is the magnetic susceptibility χ^z,

$$\chi^z = \frac{1}{k_B T L^2}\left(\langle (M^z)^2\rangle - \langle M^z\rangle^2\right), \tag{3}$$

where $\langle\cdots\rangle$ denotes the thermal average and $M^z=\Sigma_{i,j}S_{i,j}^z$ is the z-component of the total magnetization. Other observables of interest include the specific heat and the staggered magnetization. We also record typical spin configurations generated during the Monte Carlo runs in order to monitor directly microscopic properties of the system.

B. Pure (undoped) system

Before studying the influence of the disorder, it is instructive to review some basic properties of the pure system without holes. In the present context, the most relevant features of the pure model are (i) the existence, for low temperatures and fields, of a phase with long-range AFM order perpendicular to the chains, as well as (ii) the occurrence of a spin-flop transition upon applying a magnetic field along the easy axis (i.e., the z-axis).

Let us first discuss the model in zero magnetic field ($H=0$). To measure the long-range AFM order perpendicular to the chains, we define the quantity

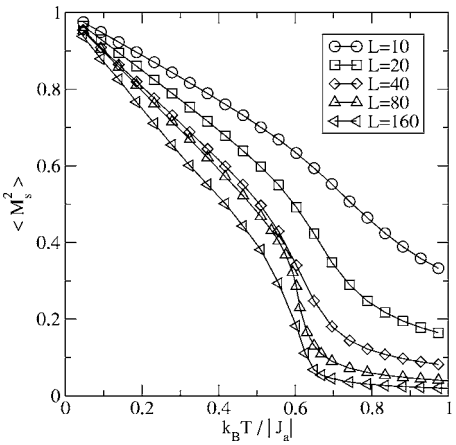

FIG. 3. Interchain order parameter, Eq. (4), of the pure model vs temperature (at $H=0$), for different system sizes L.

$$M_s^2 = \frac{1}{L}\sum_{j=1}^{L}\left(\frac{1}{L}\sum_{i=1}^{L}(-1)^i \vec{S}_{i,j}\right)^2. \quad (4)$$

Note that the expression within the parentheses is the staggered magnetization (per spin) of one column of the square lattice. We cannot simply take the difference between the total magnetizations of even and odd rows, which would be a natural candidate for the AFM order parameter, since the usual AFM structure is modified by a helical ordering of the spins along the chains, as explained below. Thus the total magnetization of each chain vanishes for $H=0$. In the fully (antiferromagnetically) ordered state, one has $M_s^2=1$.

From our simulational data (Fig. 3) we infer that a phase with long-range AFM order exists at low temperatures. The interchain order parameter M_s^2 seems to vanish continuously at a Néel temperature T_N, which we estimate as $k_BT_N/|J_a| \simeq 0.61$ by finite-size extrapolation of our data. This value is also obtained by analyzing the peak positions of the specific heat.

Taking the spin $S=1/2$ of the Cu^{2+} ions into account we obtain an estimate of $T_N=13$ K for the Néel temperature at zero field, which is reasonably close to the experimental value for $La_5Ca_9Cu_{24}O_{41}$ ($T_N=10.5$ K).[18] However, this result has to be taken with care and should only be regarded as a rough consistency check. To mention just two points, the real system is not hole-free and quantum fluctuations (absent in our classical spin model) certainly alter the value of the ordering temperature (cf. Ref. 28).

Whereas neighboring spins on adjacent chains are aligned antiferromagnetically for $T<T_N$, the spins within the chains exhibit a more complicated structure due to the competing intrachain interactions $J_{c1}>0$ and $J_{c2}<0$. At $T=0$, this structure can be found by a ground-state analysis using (and slightly generalizing) the methods described in Refs. 36 and 37. Without anisotropy ($\Delta=0$), one would obtain a simple helical ordering within each chain. In that case the spins rotate, with a constant angle α between two consecutive spins, within a plane whose orientation is fixed in space. A straightforward calculation yields $\alpha \simeq 44°$, corresponding to a wavelength of the helix of approximately eight lattice constants. The finite exchange anisotropy $\Delta>0$, however, modifies this structure. In order to minimize the anisotropy energy, the spins rotate in a plane that contains the z-axis (without anisotropy the orientation of the plane is arbitrary). Moreover, the rotation angle is not a constant, but somewhat smaller for spins in the vicinity of the z-axis. The wavelength of the modified helix, though, changes only a little as compared to the isotropic case. Such a configuration is depicted schematically in Fig. 4(a). The results of the ground-state analysis are corroborated by inspection of typical low-temperature Monte Carlo configurations. We can unambiguously identify the type of helical order shown in Fig. 4(a). The wavelength of the helix turns out to depend only weakly on temperature.

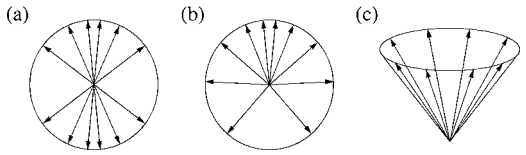

FIG. 4. Schematic representation of the (intrachain) spin configurations for (a) $H=0$, (b) $0<H<H_{sf}$, and (c) $H_{sf}<H<H_{pm}$, where H_{sf} is the spin-flop field and H_{pm} the field of the spin-flop to paramagnetic transition.

A magnetic field $H>0$ along the easy axis lifts the symmetry between the positive and negative z-direction and the system develops a finite total magnetization along the z-axis. At $T=0$, one can again find the corresponding spin configurations by a ground-state analysis. For small fields $H<H_{sf}$, where H_{sf} is the spin-flop field (see below), the analysis yields a fanlike structure [Fig. 4(b)]. At $H=H_{sf}$, this structure becomes unstable against a spin-flop phase where the spins make a finite angle with the z axis and rotate on the surface of a cone [see Fig. 4(c)]. All spins now have the same z-component, but the x- and y-components are reversed for nearest-neighbor spins on adjacent chains. This justifies calling the structure a "spin-flop phase." At $H=H_{sf}$, the z-component of the magnetization (and various other quantities) exhibit a discontinuity. For the parameters of our model, the value of the zero-temperature spin-flop field is given by $H_{sf}/|J_a| \simeq 0.70$. Upon further increasing the field the opening angle of the cone continuously shrinks to zero until at $H=H_{pm}$ all spins point along the z-axis. However, this transition from the spin-flop to the paramagnetic phase occurs at values of the magnetic field much larger than the highest fields used in the experiments and will therefore be disregarded in the following.

The above spin structures in a magnetic field $H>0$ can again be found in our finite-temperature Monte Carlo configurations. Moreover, we observe a sharp peak in the susceptibility χ^z (Fig. 5), which occurs at a field quite close to the value of the spin-flop field at $T=0$, $H_{sf}/|J_a|=0.70$ (see above). Apparently, the peak signals the (presumably first-order) transition towards the spin-flop phase. Similar anomalies are found in other quantities. The spin-flop field H_{sf} is only weakly temperature-dependent (for low temperatures).

A more detailed investigation of the phase diagram of the pure model, the nature of the various transition lines, and the behavior near possible critical and multicritical points, where

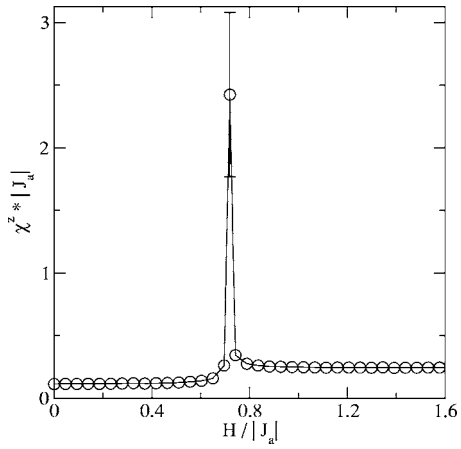

FIG. 5. Magnetic susceptibility χ^z of the pure model at fixed temperature $k_BT/|J_a|=0.25$ for a system of size $L=80$. Note the sharp spin-flop peak at $H_{\rm sf}/|J_a|\simeq 0.72$.

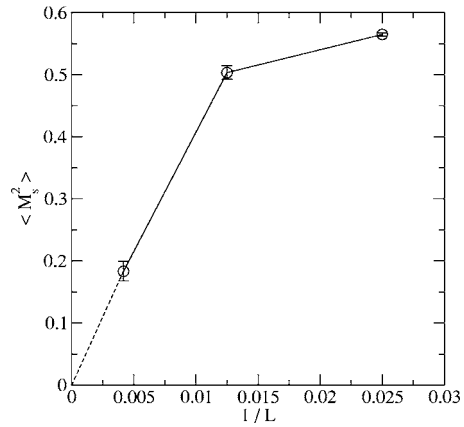

FIG. 6. Interchain order parameter, Eq. (4), for various system sizes ($L=40$, 80, and 240) at fixed temperature $k_BT/|J_a|=0.1$. For $1/L\to 0$ the order parameter seems to extrapolate to zero (dashed line), indicating the destruction of the long-range AFM order due to the quenched holes.

the different phases eventually meet, would certainly be of interest on its own but is beyond the scope of the present paper.

C. Influence of random, immobile holes

The introduction of randomly distributed, immobile holes has a drastic impact on the properties of the model. Any long-range spin order (including the AFM ordering perpendicular to the chains) gets destroyed, which leads to a smearing out of all phase transitions discussed in the previous section.

The loss of long-range order already appears in the ground-state ($T=0$). Within a modeling in terms of Ising rather than Heisenberg spins, it can be shown analytically that at $T=0$ the spin correlation function within the chains decays exponentially for large distances.[20] This is intuitively clear since the strong AFM coupling J_0 enforces an antiparallel alignment of two spins on the left and right sides of a hole. Thus the chain splits up into (ferromagnetic) fragments separated by antiphase boundaries. If the holes are distributed randomly, all long-range spin correlations along the chain are thus destroyed. For the spin correlations perpendicular to the chains an analytic treatment is much more complicated due to the frustration of the interchain interactions. The latter occurs since fragments of neighboring chains will generally be displaced against each other. In order to minimize its total energy the system will thus form additional antiphase boundaries within the chains in order to balance the competing intrachain and interchain interaction energies. In any event, one again expects an exponential decay of the spin correlations. This has been confirmed numerically.

The above mechanism for the destruction of long-range correlations may equally well apply if the Ising spins are replaced by Heisenberg spins. We have checked this by analyzing low-temperature Monte Carlo data of the AFM interchain order parameter, Eq. (4), for varying system sizes L (Fig. 6). The order parameter seems to extrapolate to zero for $L\to\infty$, indicating the absence of long-range AFM interchain order in the thermodynamic limit, as expected from the above arguments.

One should keep in mind that despite the lack of long-range order, the spins will in general still exhibit some degree of short-range ordering, which reflects the properties of the corresponding pure phases (without holes) in the various regions of the T,H-plane.

The smearing out of the phase transitions due to the presence of the randomly distributed holes can be inferred from our simulational data. For example, for $H=0$ the specific heat of the pure model exhibits a peak whose height increases with the system size L and whose position approaches the Néel temperature T_N as $L\to\infty$. For the disordered system, on the other hand, we observe a noncritical maximum, being almost size-independent for sufficiently large systems, which occurs at a "pseudo" Néel temperature $k_BT_N^{\rm ps}/|J_a|\simeq 0.58$, as compared to $k_BT_N/|J_a|\simeq 0.61$ for the pure model (see Sec. III B). Thus the Néel transition is not only smeared out but also slightly shifted towards lower temperature. In addition, the specific heat shows a small anomaly at lower temperatures, which is probably due to the incommensurability of the wavelength of the helical structures with the system size. The same conclusions are found by analyzing other quantities, such as the magnetic susceptibility.

Turning now to the (in our context) more interesting case of a nonvanishing magnetic field $H\neq 0$, we examine how the spin-flop transition of the pure system is affected by the quenched holes. Again, we find that the transition is transformed into a smooth anomaly. Whereas for the pure system the susceptibility χ^z exhibits a sharp peak at $H=H_{\rm sf}$ (cf. Fig. 5), we now observe a broad (and much smaller) maximum at a "pseudo" spin-flop field $H_{\rm sf}^{\rm ps}$ (depending on system size), see Fig. 7. The curves display some finite-size dependence for small systems. For example, the strong increase, for small system sizes, of χ^z as $H\to 0$ is weakened significantly for larger systems. For systems larger than $L=80$ the curves change only a little. The inset of Fig. 7 illustrates this for the position of the maximum, which approaches $H_{\rm sf}^{\rm ps}/|J_a|\approx 0.5$. Analogous conclusions apply to the height of the maximum,

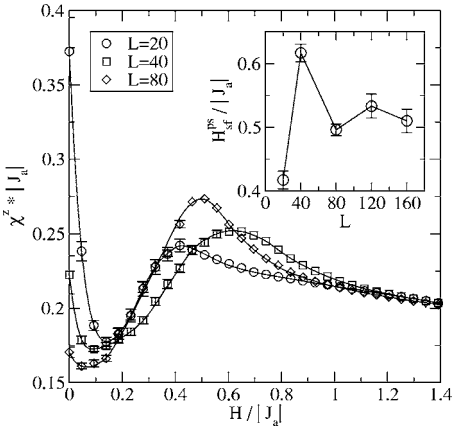

FIG. 7. Susceptibility χ^z vs magnetic field at constant temperature $k_BT/|J_a|=0.25$. The solid lines are guides to the eye. Up to 300 disorder realizations were used to generate the data. The error bars are smaller than the symbol sizes to the right of the maxima and are thus not shown there. The inset shows the position of the maximum as a function of system size.

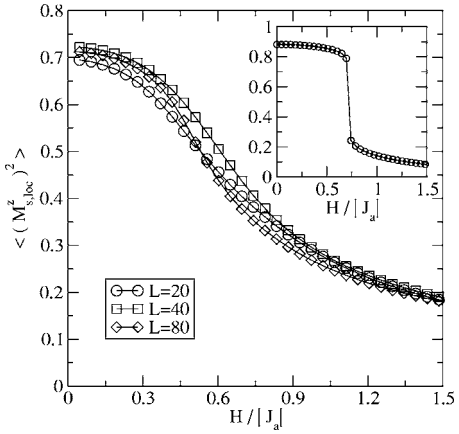

FIG. 8. Square of the z-component of the local staggered magnetization, Eq. (5), vs magnetic field at constant temperature $k_BT/|J_a|=0.25$, indicating a smooth transition between the AFM and the spin-flop phase. For the pure model, the same quantity appears to behave discontinuously at the spin-flop field (see inset). In all cases, the error bars are much smaller than the symbol size.

which quickly saturates if $L \gtrsim 80$. Thus, in the disordered case, it seems to be sufficient to simulate systems of size $L=80$ to capture the relevant properties holding in the thermodynamic limit.

A closer look at the Monte Carlo configurations reveals local spin-flop structures for $H \gtrsim H_{sf}^{ps}$, while for $H \lesssim H_{sf}^{ps}$ domains showing helically modified antiferromagnetic structures can be identified. In this sense, H_{sf}^{ps} marks a smooth crossover from the AFM phase to the spin-flop state. This qualitative picture can be corroborated by examining a suitable quantity measuring the local AFM order (see below).

For magnetic fields smaller than the spin-flop field $H \lesssim H_{sf}^{ps}$, the disorder fluctuations due to different realizations of the hole distribution are significantly larger than for $H \gtrsim H_{sf}^{ps}$. To reduce the disorder fluctuations one therefore has to average over many realizations. Since simulating many different hole distributions for all values of the field requires too much computational time, we generated a large number of up to 300 disorder realizations for lower fields only ($H < H_{sf}^{ps}$). For higher fields, 100 realizations usually turned out to be sufficient. In this way we obtained reasonably good statistics for all data points.

To provide further evidence that the broad susceptibility maximum is indeed the remnant of a smeared-out spin-flop transition, we study the square of the z-component of the local staggered magnetization, which is a measure of the degree of local AFM order perpendicular to the chains:

$$(M^z_{s,loc})^2 = \frac{1}{4L^2} \sum_{i=1}^{L} \sum_{j=1}^{L} [S^z_{i,j} - (S^z_{i-1,j} + S^z_{i+1,j})/2]^2. \qquad (5)$$

Note that the expression under the double sum is (up to a factor of 1/4) the square of the z-component of the local AFM order parameter at site (i,j). This local quantity is then averaged over the whole lattice. As exemplified in Fig. 8, $\langle (M^z_{s,loc})^2 \rangle$ drops down smoothly as one increases the magnetic field, i.e., the local AFM order along the z-direction decreases, as one expects for a transition between an AFM and a spin-flop phase. Moreover, the slope of the curve is maximal at the same field H_{sf}^{ps} where the susceptibility χ^z has its maximum (cf. Fig. 7). Note that H_{sf}^{ps} is somewhat lower than the spin-flop field $H_{sf}/|J_a| \simeq 0.70$ of the pure model. For the pure system, $\langle (M^z_{s,loc})^2 \rangle$ appears to jump at $H=H_{sf}$ (see the inset of Fig. 8).

We would like to stress that many of the above conclusions are qualitatively insensitive to details of the model like the precise values of the interaction parameters, provided that the system exhibits randomly distributed, immobile holes. In fact, we have also carried out simulations using the model proposed in Ref. 26, which was based on an interpretation of inelastic neutron scattering data for $La_5Ca_9Cu_{24}O_{41}$ (an analysis of this model, with and without mobile holes, may be found in Ref. 28). This model has a different lattice geometry, a single-ion instead of an exchange anisotropy, and quite distinct values of the interaction parameters. Moreover, we considered a simplified model with vanishing NNN coupling within the chains and a ferromagnetic NN interaction (i.e., $J_{c2}=0$ and $J_{c1}>0$). Essentially all of our conclusions concerning the smearing out of the phase transitions, which transform into (smooth) anomalies when introducing quenched holes, also hold for these modified models. On the other hand, when comparing the results of the simulations with the experimental data, the quantitative agreement seems to be most satisfying for our present model.

However, the choice of the interaction parameters certainly has an effect on the typical spin configurations within the chains. For example, for the simplified model with $J_{c2}=0$, $J_{c1}>0$ mentioned above the chains order ferromagnetically (this also applies to the model of Ref. 26). Thus in the disordered system each chain splits up into ferromagnetic fragments separated by the holes which induce antiphase boundaries. But for the present model the spins form "helical" chain fragments due to the competing intrachain interactions (see Sec. III B), and again reverse their direction across a hole. In diffraction experiments, no indications of

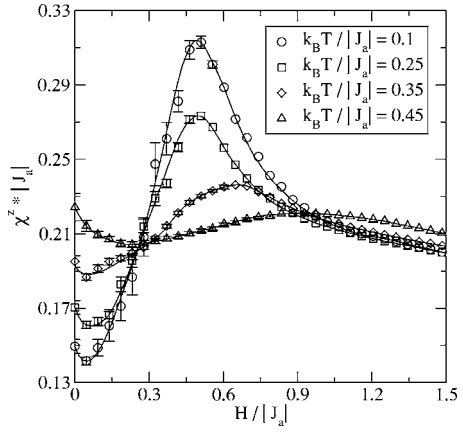

FIG. 9. Susceptibility curves for different temperatures (and system size $L=80$). As in Fig. 7, we used a varying number of up to 300 disorder realizations (depending on the value of the field) to generate the data points. The solid lines are guides to the eye.

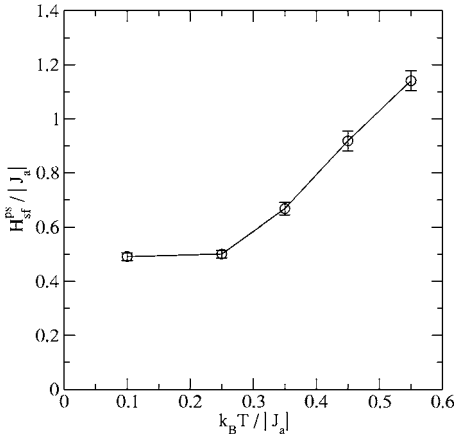

FIG. 10. Magnetic phase diagram of the model with quenched disorder. The curve shows the temperature dependence of the "pseudo" spin-flop field where the susceptibility maximum occurs (cf. Fig. 9). All data were obtained using systems of size $L=80$.

such a residual helical ordering in $La_5Ca_9Cu_{24}O_{41}$ have been found so far. One should note, however, that hints at incommensurate ordered spin structures, which could in principle be explained by the presence of a (modified) helical phase, have been reported in $La_6Ca_8Cu_{24}O_{41}$.[38] Note also that in the closely related spin-chain system Li_2CuO_2 the helical ordering is destroyed due to the anisotropy and the finite interchain coupling according to theoretical calculations.[32] Thus the existence or nonexistence of helical structures appears to be a delicate question which depends sensitively on details of the interaction and the lattice geometry (i.e., the coordination number of the interchain interaction, which is different for $La_5Ca_9Cu_{24}O_{41}$ and Li_2CuO_2).

Plotting the susceptibility curves for various temperatures (Fig. 9) allows us to draw a more detailed comparison with the experimental magnetization measurements. The temperature dependence of both the position and the height of the spin-flop anomaly resemble the experimental data which will be presented in Sec. IV (Fig. 11) quite well.

Finally, we depict the "magnetic phase diagram" of our model in Fig. 10, i.e., the dependence of the "pseudo" spin-flop field H^{ps}_{sf} on temperature. Again, we find qualitative agreement with the upper line B_2 of the experimental phase diagram (Fig. 11). If one converts the theoretical values for H^{ps}_{sf} into physical units, taking the spin value $S=1/2$ of the Cu^{2+} ions and the correct g-factors[15] properly into account, we obtain a "pseudo" spin-flop field of approximately 9 T for a temperature of $k_BT/|J_a|=0.1$. This compares reasonably well with the experimental values. An even better agreement may be reached by fine-tuning of the interaction parameters (whose precise values are not known yet), taking into account quantum effects, or allowing for a (partial) mobility of the holes.

Summarizing, the above findings corroborate the idea that the experimentally observed broad anomaly in the susceptibility curves can indeed be understood as a disorder phenomenon due to randomly distributed, quasistatic holes, which lead to a destruction of the long-range AFM order and, correspondingly, to a smearing-out of the spin-flop transition.

IV. EXPERIMENTAL RESULTS ON THE "PSEUDO SPIN-FLOP PEAK"

In order to test the numerical predictions of the preceding section, we here present some of our experimental data on the magnetic properties of the lightly hole-doped spin chains in $La_x(Ca,Sr)_{14-x}Cu_{24}O_{41}$. We studied single crystals of approximately 0.2 cm^3, grown by the floating zone technique.[39] For the magnetization measurements a vibrating sample magnetometer (VSM) was used. The measurements were performed in magnetic fields up to 16 T. The fields were applied either parallel to the chain direction (c axis) or per-

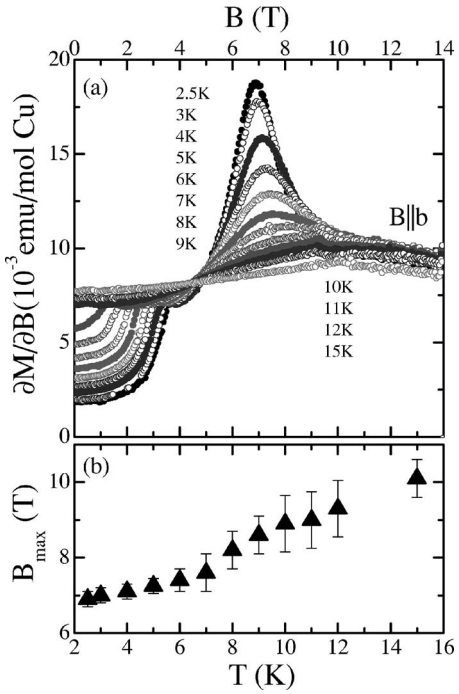

FIG. 11. Susceptibility of $La_{5.2}Ca_{8.8}Cu_{24}O_{41}$ vs magnetic field $B\|b$ parallel to the easy axis for different temperatures, (a), and position of the maximum in (a) vs temperature, (b).

pendicular to the CuO_4 plaquettes of the CuO_2 chains, i.e., along the easy magnetic axis (b axis).

Figure 11(a) shows the susceptibility of $La_{5.2}Ca_{8.8}Cu_{24}O_{41}$ vs magnetic field along the b-axis, at different temperatures up to 15 K $> T_N = 10.5$ K. The sharp anomaly at B_1, which signals the melting of the long-range spin order, is visible for all temperatures below T_N. In contrast to the melting of the spin order, the anomaly at B_2 is still present for $T > T_N$, where only short-range spin correlations exist. This fact agrees with the observation that at $T = 2.5$ K the anomaly occurs at fields $B > B_1$, where also only short-range spin order does exist. Upon heating, the anomaly is shifted to higher fields. Moreover, the peak both shrinks and broadens drastically at higher temperatures. Comparing the data in Fig. 11(a) with those in Fig. 9 illustrates the similarities between the experimental data and the numerical results. The broad peak at B_2 is well-described by the model calculations, which strongly reinforces the approach presented in Sec. III.

The temperature dependence of the "pseudo" spin-flop transition in $La_{5.2}Ca_{8.8}Cu_{24}O_{41}$ is summarized in Fig. 11(b). Qualitatively, the presence of the broad anomaly B_2 indicates short-range spin correlations up to 15 K. The temperature dependence of the peak maximum depends roughly linearly on the temperature, in agreement with the numerical findings (Fig. 10). At (7 ± 1) K, the curvature of $B_2(T)$ slightly changes, which again resembles the numerical results.

V. CONCLUSION AND OUTLOOK

We have presented measurements of the magnetic properties of the anisotropic spin chains in lightly hole-doped $La_x(Ca,Sr)_{14-x}Cu_{24}O_{41}$, $x \gtrsim 5$. The experiments suggest that for fields $B \gtrsim 4$ T the system is characterized by short-range AFM spin order and quasistatic charge disorder. The susceptibility as a function of the magnetic field B (applied along the easy axis) shows a broad anomaly instead of a sharp peak, as one would have expected if the system underwent a spin-flop transition (and as one indeed observes in the related, but hole-free spin chain compound Li_2CuO_2, see Ref. 22). In order to understand these findings theoretically, we have carried out Monte Carlo simulations of an anisotropic classical Heisenberg model with quenched holes. Our numerical data show that the spin-flop transition of the pure model is smeared out upon introducing quenched holes. The susceptibility curves at fixed temperature exhibit broad peaks and resemble the experimental data quite well. At low temperatures, the peak occurs at a field value slightly below the corresponding spin-flop field of the pure system. Furthermore, the peak position increases with temperature, similarly as it is observed in the experiments. Taken together, our numerical studies corroborate the idea that the broad anomaly in the experimental susceptibility curves is essentially a signature of the disorder due to quasistatic holes.

Nonetheless, there remain several challenging questions for future (experimental and theoretical) work. One of them concerns the possible mechanisms for the pinning of the holes, which would explain the occurrence of quasistatic (quenched) charge disorder. While the destruction of the stripe-ordered phase by an effective, field-induced attraction of the holes (as proposed in Refs. 20 and 22) obviously requires a certain mobility of the holes, the existence of the broad anomaly in the susceptibility seems to suggest that pinning might play an important role to understand the high-field behavior ($B > B_1$). If one assumes the holes to move freely along the chains, the theoretical models predict a clustering of the holes upon increasing the field and no broad anomaly in the susceptibility occurs (see the discussion in Ref. 28). Thus one may speculate that as the field becomes large enough ($B > B_1$) and the holes start to move around, they get trapped at (randomly distributed) pinning centers and then stay more or less immobile.

Closely related to the pinning of the holes is the possible influence of the Coulomb interaction, which has been neglected in the theoretical models so far. The Coulomb repulsion of the holes destabilizes the above-mentioned clustered structures and would tend to distribute the holes more uniformly across the system. It is unclear, however, whether inclusion of the Coulomb interaction between the holes alone would suffice to predict the existence of quasistatic disorder for fields $B > B_1$. It might also be necessary to take the interaction with the La^{3+} and Ca^{2+} ions into account. Due to their different charges and ionic radii, these might introduce additional disorder into the system which may turn out to be important for an understanding of the pinning of the holes.

ACKNOWLEDGMENTS

We thank J. M. Tranquada for a useful discussion. This work was supported by the Deutsche Forschungsgemeinschaft (DFG) within SPP 1073 (BU 887/1-3). W.S., M.H., and R.K. gratefully acknowledge financial support by the Deutsche Forschungsgemeinschaft under Grants No. SE 324/4 and KL 1824/1-1, respectively.

[1] S. Kivelson, I. Bindloss, E. Fradkin, V. Oganesyan, J. Tranquada, A. Kapitulnik, and C. Howald, Rev. Mod. Phys. **75**, 1201 (2003).

[2] J. M. Tranquada, D. J. Buttrey, V. Sachan, and J. E. Lorenzo, Phys. Rev. Lett. **73**, 1003 (1994).

[3] P. Wochner, J. M. Tranquada, D. J. Buttrey, and V. Sachan, Phys. Rev. B **57**, 1066 (1998).

[4] B. J. Sternlieb, J. P. Hill, U. C. Wildgruber, G. M. Luke, B. Nachumi, Y. Moritomo, and Y. Tokura, Phys. Rev. Lett. **76**, 2169 (1996).

[5] M. Takigawa, N. Motoyama, H. Eisaki, and S. Uchida, Phys. Rev. B **57**, 1124 (1998).

[6] C. Hess, H. ElHaes, B. Büchner, U. Ammerahl, M. Hücker, and A. Revcolevschi, Phys. Rev. Lett. **93**, 027005 (2004).

[7] R. Klingeler, N. Tristan, B. Büchner, M. Hücker, U. Ammerahl, and A. Revcolevschi, Phys. Rev. B **72**, 184406 (2005).

[8] P. Horsch, M. Sofin, M. Mayr, and M. Jansen, Phys. Rev. Lett. **94**, 076403 (2005).
[9] D. Akahoshi, M. Uchida, Y. Tomioka, T. Arima, Y. Matsui, and Y. Tokura, Phys. Rev. Lett. **90**, 177203 (2003).
[10] J. Burgy, M. Mayr, V. Martin-Mayor, A. Moreo, and E. Dagotto, Phys. Rev. Lett. **87**, 277202 (2001).
[11] E. Dagotto, Science **309**, 257 (2005).
[12] G. Alvarez, M. Mayr, A. Moreo, and E. Dagotto, Phys. Rev. B **71**, 014514 (2005).
[13] R. S. Eccleston, M. Uehara, J. Akimitsu, H. Eisaki, N. Motoyama, and S. I. Uchida, Phys. Rev. Lett. **81**, 1702 (1998).
[14] V. Yu. Yushankhai and R. Hayn, Europhys. Lett. **47**, 116 (1999).
[15] V. Kataev, K.-Y. Choi, M. Grüninger, U. Ammerahl, B. Büchner, A. Freimuth, and A. Revcolevschi, Phys. Rev. Lett. **86**, 2882 (2001).
[16] L. P. Regnault, J. P. Boucher, H. Moudden, J. E. Lorenzo, A. Hiess, U. Ammerahl, G. Dhalenne, and A. Revcolevschi, Phys. Rev. B **59**, 1055 (1999).
[17] U. Ammerahl, B. Büchner, L. Colonescu, R. Gross, and A. Revcolevschi, Phys. Rev. B **62**, 8630 (2000).
[18] M. Matsuda, K. M. Kojima, Y. J. Uemura, J. L. Zarestky, K. Nakajima, K. Kakurai, T. Yokoo, S. M. Shapiro, and G. Shirane, Phys. Rev. B **57**, 11467 (1998).
[19] U. Ammerahl, B. Büchner, C. Kerpen, R. Gross, and A. Revcolevschi, Phys. Rev. B **62**, R3592 (2000).
[20] W. Selke, V. L. Pokrovsky, B. Büchner, and T. Kroll, Eur. Phys. J. B **30**, 83 (2002).
[21] T. Kroll, R. Klingeler, J. Geck, B. Büchner, W. Selke, M. Hücker, and A. Gukasov, J. Magn. Magn. Mater. **290-291**, 306 (2005).
[22] R. Klingeler, Ph.D. thesis, RWTH Aachen, 2003.
[23] M. Holtschneider and W. Selke, Phys. Rev. E **68**, 026120 (2003).
[24] M. Holtschneider, W. Selke, and R. Leidl, J. Magn. Magn. Mater. **290-291**, 326 (2005).
[25] W. Selke, M. Holtschneider, and R. Leidl, Condens. Matter Phys. **8**, 15 (2005).
[26] M. Matsuda, K. Kakurai, J. E. Lorenzo, L. P. Regnault, A. Hiess, and G. Shirane, Phys. Rev. B **68**, 060406(R) (2003).
[27] A. Gukasov (unpublished).
[28] R. Leidl and W. Selke, Phys. Rev. B **70**, 174425 (2004).
[29] Y. Mizuno, T. Tohyama, S. Maekawa, T. Osafune, N. Motoyama, H. Eisaki, and S. Uchida, Phys. Rev. B **57**, 5326 (1998).
[30] R. Leidl and W. Selke, Phys. Rev. B **69**, 056401 (2004).
[31] M. Matsuda, T. Yosihama, K. Kakurai, and G. Shirane, Phys. Rev. B **59**, 1060 (1999).
[32] S.-L. Drechsler, J. Richter, J. Málek, A. S. Moskvin, R. Klingeler, and H. Rosner, J. Magn. Magn. Mater. **290-291**, 345 (2005).
[33] R. Klingeler, B. Büchner, K.-Y. Choi, V. Kataev, U. Ammerahl, A. Revcolevschi, and J. Schnack, Phys. Rev. B **73**, 014426 (2006).
[34] Y. Mizuno, T. Tohyama, and S. Maekawa, Phys. Rev. B **60**, 6230 (1999).
[35] C. de Graaf, I. de P. R. Moreira, F. Illas, Ò. Iglesias, and A. Labarta, Phys. Rev. B **66**, 014448 (2002).
[36] T. Nagamiya, K. Nagata, and Y. Kitano, Prog. Theor. Phys. **27**, 1253 (1962).
[37] J. M. Robinson and P. Erdös, Phys. Rev. B **2**, 2642 (1970).
[38] M. Matsuda, K. Katsumata, T. Yokoo, S. M. Shapiro, and G. Shirane, Phys. Rev. B **54**, R15626 (1996).
[39] U. Ammerahl and A. Revcolevschi, J. Cryst. Growth **197**, 825 (1999).